Distributions of Microbial Activities in Deep Subseafloor Sediments

Steven D'Hondt,[1]* Bo Barker Jørgensen,[1] D. Jay Miller,[1] Anja Batzke,[2] Ruth Blake,[1] Barry A. Cragg,[1] Heribert Cypionka,[1] Gerald R. Dickens,[1] Timothy Ferdelman,[1] Kai-Uwe Hinrichs,[1] Nils G. Holm,[1] Richard Mitterer,[1] Arthur Spivack,[1] Guizhi Wang,[3] Barbara Bekins,[1] Bert Engelen,[2] Kathryn Ford,[1] Glen Gettemy,[1] Scott D. Rutherford,[4] Henrik Sass,[2] C. Gregory Skilbeck,[1] Ivano W. Aiello,[1] Gilles Guèrin,[1] Christopher H. House,[1] Fumio Inagaki,[1] Patrick Meister,[1] Thomas Naehr,[1] Sachiko Niitsuma,[1] R. John Parkes,[1] Axel Schippers,[1] David C. Smith,[1] Andreas Teske,[1] Juergen Wiegel,[1] Christian Naranjo Padilla,[1] Juana Luz Solis Acosta[1]

Diverse microbial communities and numerous energy-yielding activities occur in deeply buried sediments of the eastern Pacific Ocean. Distributions of metabolic activities often deviate from the standard model. Rates of activities, cell concentrations, and populations of cultured bacteria vary consistently from one subseafloor environment to another. Net rates of major activities principally rely on electron acceptors and electron donors from the photosynthetic surface world. At open-ocean sites, nitrate and oxygen are supplied to the deepest sedimentary communities through the underlying basaltic aquifer. In turn, these sedimentary communities may supply dissolved electron donors and nutrients to the underlying crustal biosphere.

Microbial life is widespread in the marine sediments that cover more than two-thirds of Earth's surface. Intact cells (*1*) and intact membrane lipids (*2*, *3*) provide evidence of prokaryotic populations in sediments as deep as 800 m below the seafloor (mbsf). Prokaryotic activity, in the form of sulfate (SO_4^{2-}) reduction and/or methanogenesis, occurs in sediments throughout the world ocean (*4*). The prokaryotes of subseafloor sediments have been estimated to constitute as much as one-third of Earth's total living biomass (*5*).

Despite the ubiquity of life in subseafloor sediments, little is known about it. The diversity of its metabolic activities, the composition of its communities, and the nature of its variation from one environment to another are largely unknown. Its relationship to the photosynthetic surface world is not fully understood. Its relationship to the deeper world of the underlying basaltic crust has not been tested.

To explore life in deeply buried marine sediments, we undertook Ocean Drilling Program (ODP) Leg 201. The expedition sites are located in the equatorial Pacific Ocean and on the continental margin of Peru (Fig. 1) (*6*). These sites are typical of subsurface environments that exist throughout most of Earth's ocean. Their water depths range from 150 m on the Peru Shelf to 5300 m in the Peru Trench. The sampled sediments ranged in subseafloor depth from 0 to 420 m, in temperature from 1° to 25°C, and in age from 0 to 35 million years ago (Ma) (*6*, *7*). Prokaryotic cells occur throughout the sampled sediment column at every site (Fig. 1) (*8*).

Diversity of metabolic activities. Dissolved electron acceptors such as SO_4^{2-} and nitrate (NO_3^-) exhibit subsurface depletion, whereas dissolved metabolic products such as dissolved inorganic carbon ($DIC = CO_2 + HCO_3^- + CO_3^{2-}$), ammonia ($\Sigma NH_3 = NH_3 + NH_4^+$), sulfide ($\Sigma H_2S = H_2S + HS^-$), methane ($CH_4$), manganese [inferred to be Mn(II)], and Fe [inferred to be Fe(II)] consistently exhibit concentration maxima deep in the drilled sediment columns (e.g., Fig. 1). These concentration profiles indicate that biologically catalyzed reactions consume and release metabolites deep in the sediment column at all of the sites. The microbial processes implicit in Fig. 1 include organic carbon oxidation, ammonification, methanogenesis, methanotrophy, sulfate reduction, and manganese reduction. Other processes that occur in these sediments include iron reduction and the production and consumption of formate, acetate, lactate, hydrogen, ethane, and propane (*6*).

These activities are unexpectedly diverse. The interstitial water chemistry of shallow marine sediments generally exhibits a predictable zonation, with peak concentrations of dissolved products from different redox processes [Mn(II), Fe(II), ΣH_2S, and CH_4] present at successively greater sediment depths (*9*–*12*). This succession of redox zones has been ascribed to competition between metabolic pathways; electron-accepting reactions that yield successively less negative standard free energies are hypothesized to predominate at successively greater depths because electron acceptors with higher free energy yields are depleted at shallower depths [e.g., (*9*, *11*)]. In shallow marine sediments that exhibit this zonation, terminal electron acceptors ultimately enter the sediment from the overlying ocean. As the reduced products from below enter successively shallower zones of SO_4^{2-}, Fe(III), Mn(IV), NO_3^-, and O_2 reduction, vertical cascades of electron-accepting processes are sustained (*11*). For example, O_2 may be used to oxidize Mn(II) to Mn(IV), which can oxidize Fe(II) to Fe(III), which might oxidize reduced sulfur, which ultimately could oxidize hydrogen or organic carbon.

In many respects, dissolved chemical profiles of Leg 201 sites exhibit this standard zonation. However, they also depart from it in four important ways. First, at site 1229, the introduction of dissolved SO_4^{2-} from below reverses the standard redox zonation by sustaining a zone with abundant SO_4^{2-} beneath a sulfate-depleted methane-rich zone (Fig. 2). At this site and at nearby site 1228, SO_4^{2-} is introduced at depth by upward diffusion from ancient brine (*6*). This deep brine is present along much of the Peru Shelf (*13*). At sites 1225 and 1226, SO_4^{2-} similarly diffuses upward into the deepest sediments from water circulating through the underlying basaltic aquifer. Sulfate is supplied to the deepest sediments in this manner throughout much of the eastern equatorial Pacific (*14*).

Second, at some sites, the expected zonation is locally reversed by the appearance of

[1]Ocean Drilling Program Leg 201 Shipboard Scientific Party. [2]Institut für Chemie und Biologie des Meeres, Universität Oldenburg, D-26111 Oldenburg, Germany. [3]University of Rhode Island Graduate School of Oceanography, Narragansett, RI 02882, USA. [4]Department of Environmental Science, Roger Williams University, Bristol, RI 02809, USA.

*To whom correspondence should be addressed at NASA Astrobiology Institute, University of Rhode Island Graduate School of Oceanography, South Ferry Road, Narragansett, RI 02882, USA. E-mail: dhondt@gso.uri.edu

large peaks in dissolved Mn and Fe concentrations far below the seafloor (e.g., Figs. 1 to 3). Such midcolumn peaks demonstrate that, in discrete intervals, concentrations of buried iron- and manganese-bearing minerals can be high enough and their rates of dissolution and reduction slow enough to continue long after metabolic activities with lower standard free energies have become predominant in shallower sediments.

Third, subsurface CH_4 maxima occur within the sediments of all Leg 201 sites, including the open-ocean sites where dissolved SO_4^{2-} concentrations are high (*6*) (Fig. 1). Similar maxima have recently been identified at many other open-ocean sites (*4*, *15*). They indicate that methanogenesis occurs deep beneath the seafloor in most, perhaps all, marine sediments, regardless of SO_4^{2-} availability. This result indicates that methanogenesis occurs long before electron acceptors that yield higher standard free energies have been depleted.

The fourth important departure occurs only at the open-ocean sites, where the succession of redox zones that extends from the seafloor to greater depths is mirrored by a similar succession that extends upward from the basement-sediment interface (Fig. 3). At sites 1225 and 1231, relatively high concen-

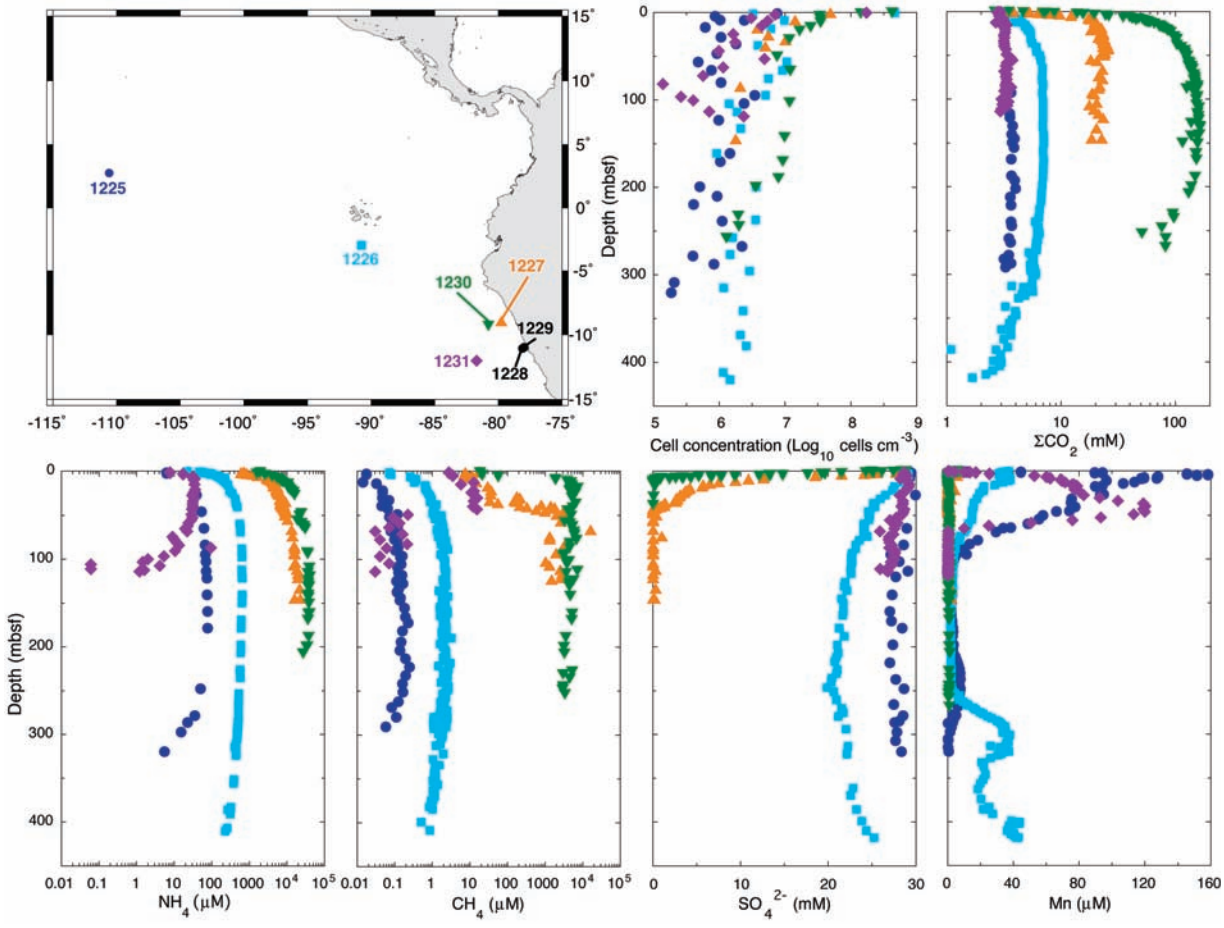

Fig. 1. Map of Leg 201 sites and concentration profiles of several dissolved chemical species at five of the sites (*17*). At sites 1225, 1226, and 1231, the deepest sample was taken just above the basaltic basement.

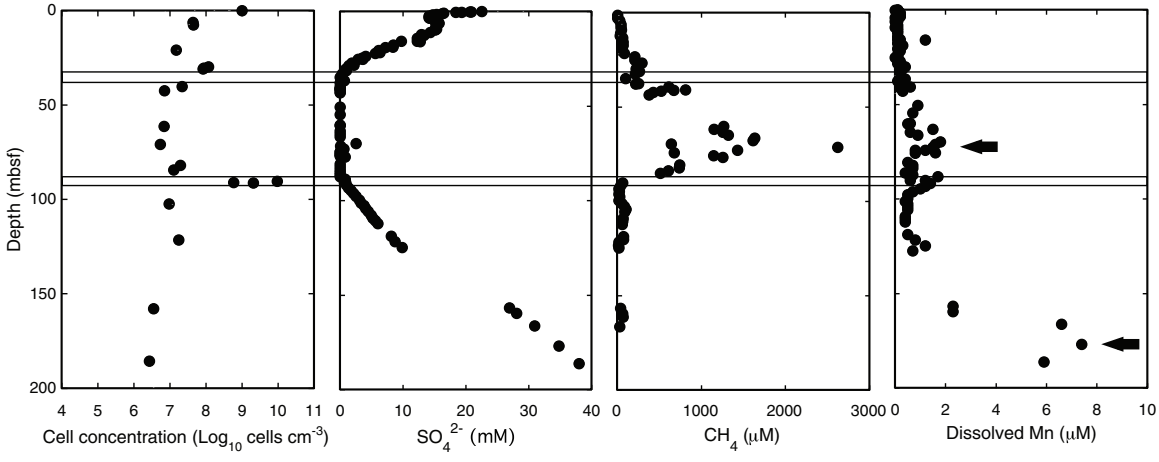

Fig. 2. Concentration profiles of cells and some dissolved chemicals at site 1229 (*17*). White bands mark sulfate-methane transition zones. Arrows mark midcolumn peaks in dissolved Mn concentrations.

trations of NO_3^- and traces of O_2 were discovered at the base of the sediment column (*16*, *17*). This NO_3^- and O_2 presumably enters the sediments from oxic water circulating through the underlying basaltic basement.

A local peak in dissolved Mn occurs just above this deep nitrate-reducing zone at both sites 1225 and 1231 (Fig. 3). A similar peak occurs in the basal sediments of site 1226. At all three sites, these Mn concentration maxima are stratigraphically overlain by maxima in dissolved Fe concentrations. These Mn and Fe maxima mark successive intervals of Mn and Fe reduction.

The deep occurrences of successive O_2, NO_3^-, Mn, and Fe redox zones at open-ocean sites have three immediate implications. First, the transport of O_2 and NO_3^- through the underlying basaltic aquifer sustains aerobic and nitrate-reducing prokaryotic communities in the deepest (11 to 35 Ma) sediments of these sites, although anaerobic communities are active in the overlying sediment. Second, this deep introduction of NO_3^- and O_2 may cause Mn and Fe oxidation fronts and thereby sustain continued Mn and Fe cycling at the base of the sediment column. Third, respiration along the flow path through the underlying basalts is insufficient to strip O_2 and NO_3^- from the circulating water. Respiration in these basaltic aquifers may be limited by electron donor availability (*18*).

These discoveries indicate that the energy-yielding activities of deep subseafloor sedimentary ecosystems are far more diverse than can be predicted from the standard redox zonation of shallow marine sediments. Although unexpected, the reversed redox successions of the deepest open-ocean sediments are consistent with the hypothesis that electron-accepting pathways with successively lower standard free energies predominate at successively greater distances from a source of oxic water. The reversed subseafloor succession of site 1229 (from methanogenesis to sulfate reduction) is similarly consistent with this hypothesis.

The occurrence of methanogenesis in sulfate-replete porewaters and the occurrences of Mn and Fe reduction in deep methanogenic zones and deep sulfate-reducing zones require different explanation(s) than the reversed redox zones. There are at least three possible explanations of these occurrences: (i) The organisms that undertake these different processes may rely on noncompetitive substrates (different electron donors) in deep marine sediments; (ii) organisms that rely on electron-accepting pathways with higher standard free energies may have higher energy requirements than organisms that rely on pathways with lower standard free energy yields; or (iii) the in situ free energies of these reactions may differ greatly from their standard free energies (for example, all of these reactions may yield similar free energies in deep subseafloor sediments where they co-occur). Whichever explanation ultimately applies, subseafloor occurrences of many electron-accepting activities cannot be predicted by simple extrapolation of the shallow marine redox zonation to sediments at greater depths.

Rates of electron-accepting activities. At steady state, fluxes of SO_4^{2-} and NO_3^- into a sediment column are respectively equal to net reduction rates of SO_4^{2-} and NO_3^- within that column. Also at steady state, the minimum rate of metal (Mn or Fe) reduction is equal to the flux of the dissolved metal from zones of net reduction (marked by local concentration peaks) to zones of net precipitation or oxidation (marked by concentration minima) (*19*).

Biogeochemical flux models based on concentration data and sediment physical properties were used to quantify rates of these electron-accepting activities at most Leg 201 sites (Table 1) (*17*, *19*). Net rates of SO_4^{2-} reduction in subseafloor sediments (>1.5 mbsf), net fluxes of ΣH_2S out of those sediments, and estimated Fe reduction rates within the sediments are much higher at the ocean-margin sites than at the open-ocean sites. In contrast, estimated Mn reduction rates and net NO_3^- reduction rates in the subsurface sediments (from >1.5 mbsf to the base of the drilled sediments) are higher at the open-ocean sites than at the ocean-margin sites. These net NO_3^- reduction rates entirely result from the introduction of NO_3^- from the underlying basaltic aquifers.

These rates of subseafloor activities vary predictably from open-ocean sites to ocean-margin sites (Table 1). At each site, the predominant energy-yielding pathways may be a function of total electron-accepting activity. For example, if the electron donor is C(0) for electron-accepting reactions, carbon oxidation by net SO_4^{2-} reduction appears to greatly outpace carbon oxidation by metal (Mn and Fe) reduction at the high-activity ocean-margin sites and the most active open-ocean site (Table 1) (*20*). In contrast, at the open-ocean site where net activities are lowest (site 1231), SO_4^{2-} reduction is not detectable and net respiration in sediments deeper than 1.5 mbsf may principally rely on reduction of Mn(IV) and Fe(III).

Biogeochemical linkages to the surface world and to life in underlying aquifers. The activities in Table 1 ultimately rely on electron acceptors from the photosynthetically oxidized surface world. O_2, NO_3^-, and SO_4^{2-} ultimately enter these sediments by diffusing down past the seafloor and, at the open-ocean sites, by transport upward from seawater flowing through the underlying basalts. The oxidized Mn and Fe were originally introduced to the sediments by deposition of Mn and Fe at the seafloor.

The activities in Table 1 probably also principally rely on electron donors from the photosynthetically oxidized surface world. The ultimate electron donors for subsurface eco-

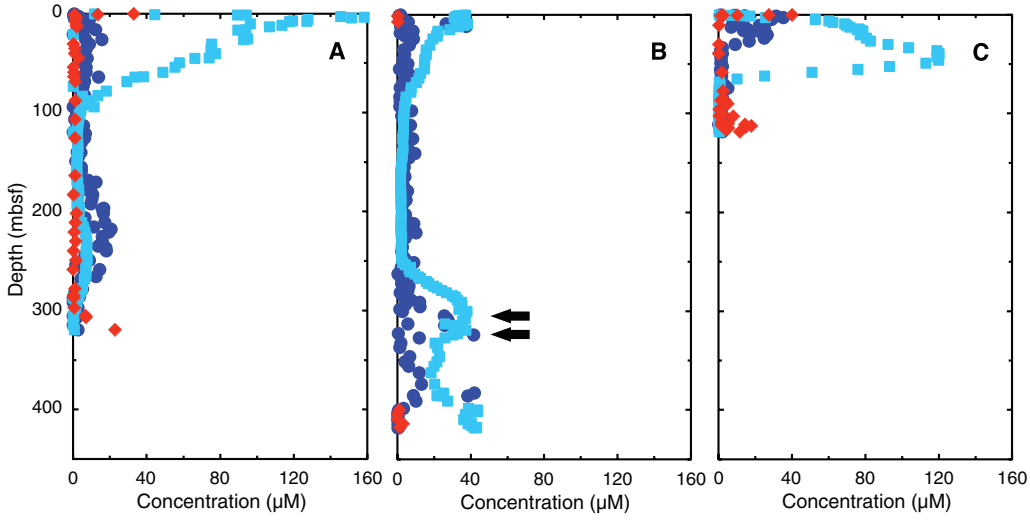

Fig. 3. Dissolved concentration profiles of NO_3^- (red diamonds), Mn (light blue squares), and Fe (dark blue circles) at open-ocean sites 1225 (**A**), 1226 (**B**), and 1231 (**C**). Arrows mark midcolumn peaks in dissolved concentrations of Mn and Fe at site 1226. At each site, the deepest sample was taken just above the basaltic basement.

systems have been hypothesized to include buried organic matter from the surface world (*9*, *10*), reduced minerals [such as Fe(II)-bearing silicates] (*21*, *22*), and thermogenic CH_4 from deep within Earth (*23*). Comparison of our subseafloor carbon oxidation estimates to published estimates of organic burial rates (*24*) suggests that buried organic carbon from the overlying photosynthetic world is abundant enough to fuel most or all of the estimated electron-accepting activities (Table 1).

The role of reduced minerals cannot be directly assessed with our data. However, thermodynamic considerations preclude oxidation of Fe(II) or Mn by Fe(III) or SO_4^{2-}. Consequently, reduced Fe and Mn are unlikely to be important subseafloor electron donors at any sites where SO_4^{2-} or Fe(III) is the principal electron acceptor. In the sediments of site 1231, where Mn(IV) appears to be the principal electron acceptor, Fe(II) may be an important electron donor.

Our data clearly indicate that activity in the sediments of our open-ocean sites is not fueled by thermogenic CH_4 from deep within Earth. Maximum concentrations in the middle of each open-ocean sediment column and minimum concentrations near the sediment-basement interface (Fig. 1) indicate that biogenic CH_4 and ΣNH_3 are produced deep in these sediments, and, at sites where chemical transport is dominantly diffusive, actually migrate downward toward the underlying basalts. In this manner, the deep sedimentary communities may provide electron donors and biologically accessible nitrogen to communities in the underlying basaltic aquifers.

Environmental variation in cell abundance and cultured isolates of subseafloor sedimentary communities. Cell concentrations vary with metabolic reaction rates and metabolic product concentrations from site to site (Fig. 1). For example, cell concentrations are highest at sites where concentrations of metabolic products (ΣNH_3, CH_4, DIC) and net rates of SO_4^{2-} reduction and Fe reduction are highest, and cell concentrations are lowest at sites where these rates and metabolic product concentrations are lowest (Fig. 1 and Table 1). The open-ocean sites contained some of the lowest average cell concentrations ever observed in deep-sea sediments, whereas sediments recovered from the Peru Shelf contained the highest concentrations ever observed beneath the seafloor (Fig. 2).

Cell concentration profiles are also closely related to dissolved reactant distributions within individual sites. For example, at site 1229, high cell concentrations occur in subseafloor sulfate-methane transition zones (Fig. 2). Diffusion of the two reactants (SO_4^{2-} and CH_4) to these zones provides an interface of high biochemical energy supply. At one such zone (92 mbsf), this interface supports cell densities that are an order of magnitude higher than at the seafloor (Fig. 2).

Bacteria were successfully cultured and isolated from multiple depths at every site (Table 2) (*17*). These cultures indicate that living bacteria are present throughout the entire range of subseafloor depths sampled by Leg 201 (1 to 420 mbsf) (Table 2). As assessed from the 16*S* ribosomal RNA (rRNA) genes of 168 isolates, these bacteria belong to at least six distinct lineages (Table 2) (*17*). Most of these isolates are closely related to known marine organisms. Others are more distant from known organisms. Most strikingly, the 16*S* gene of one isolate from open-ocean site 1225 differs from the 16*S* gene of its nearest known relative (a member of the Bacteroidetes) by 14% (Table 2). In combination with the recent discovery of deeply rooted but previously unknown archaeal 16*S* gene sequences in subseafloor sediments of site 1231 (*25*), this isolate demonstrates that previously undiscovered prokaryotes exist in deep subseafloor sediments of the open ocean.

Although the cultured bacteria constitute only a small fraction of the total cell count in each sample (up to 0.1%), these results hint of consistent patterns in the community composition of subsurface sediments. Some lineages appear to be cosmopolitan members of subseafloor sedimentary communities. The most commonly cultured taxa are Firmicutes that are most closely related to the spore-forming bacterium *Bacillus firmus* and α-Proteobacteria that are most closely related to *Rhizobium radiobacter*. These taxa were often recovered from open-ocean sediments with abundant dissolved SO_4^{2-} and little CH_4 (Table 2). They were also often recovered from ocean-margin sediments with abundant CH_4 and no dissolved SO_4^{2-}. Close relatives of *R. radiobacter* have also been recently isolated from Mediterranean subseafloor sediments (*26*). Recent surveys of archaeal 16*S* genes in subseafloor sediments suggest that some archaeal lineages [the Deep-Sea Archaeal Group and the Marine Benthic Group A] are similarly cosmopolitan members of subseafloor sedimentary communities (*27*).

Other lineages appear to be more selective in their subseafloor environmental affinities. For example, cultured γ-Proteobacteria were consistently found at ocean-margin sites (Table 2), where concentrations of organic matter, cell concentrations, and net metabolic rates are high. However, they were rarely found at open-ocean sites, where organic concentrations, cell counts, and net metabolic rates are low. In contrast, Actinobacteria were most consistently found in sulfate-reducing sediments of the open-ocean sites (sites 1225, 1226, and 1231) and ocean-margin site 1227.

In short, subseafloor sedimentary communities contain some taxa that inhabit a

Table 1. Estimated reduction rates and carbon oxidation equivalents at ODP Leg 201 sites. BDL, below detection limit; ND, not determined.

Leg 201 location	Water depth (m below sea level)	Net NO_3^- reduction (mol cm^{-2} year^{-1})	Estimated Mn reduction (mol cm^{-2} year^{-1})	Estimated Fe reduction (mol cm^{-2} year^{-1})	Net SO_4^{2-} reduction (mol cm^{-2} year^{-1})	ΣH_2S flux out of sediment column (mol cm^{-2} year^{-1})	Potential C oxidation by net NO^{3-} reduction (mol cm^{-2} year^{-1})	Potential C oxidation by estimated Mn(IV) reduction (mol cm^{-2} year^{-1})	Potential C oxidation by estimated Fe(III) reduction (mol cm^{-2} year^{-1})	Potential C oxidation by net SO_4^{2-} reduction (mol cm^{-2} year^{-1})	Organic carbon burial rate (*24*) (mol cm^{-2} year^{-1})
Peru margin sites											
Shelf site 1227	427	BDL	2.2×10^{-11}	1.0×10^{-7}*	0.9×10^{-6}	-0.7×10^{-6}	BDL	1.1×10^{-11}	2.5×10^{-8}	1.8×10^{-6}	3.1×10^{-6}
Slope site 1230	5086	ND	1.4×10^{-10}	2.5×10^{-7}*	2.5×10^{-6}	-2.0×10^{-6}	ND	0.7×10^{-10}	6.3×10^{-8}	5.0×10^{-6}	3.1×10^{-6}
Open Pacific sites											
Equatorial site 1225	3760	1.3×10^{-9}	2.9×10^{-8}	1×10^{-8}*	1.9×10^{-8}	BDL	1.6×10^{-9}	1.5×10^{-8}	2.5×10^{-9}	3.8×10^{-8}	4.5×10^{-7}
Equatorial site 1226	3297	ND	5.9×10^{-9}	7×10^{-8}*	1.4×10^{-7}	-1.3×10^{-9}	ND	3.0×10^{-9}	1.8×10^{-8}	2.8×10^{-7}	4.6×10^{-7}
Peru Basin site 1231	4813	8.0×10^{-9}	6.1×10^{-8}	3.9×10^{-8}	BDL	BDL	1.0×10^{-8}	3.0×10^{-8}	1.0×10^{-8}	BDL	9.4×10^{-7}

*Inferred from net S burial. Assumes all buried S goes to FeS_2.

Table 2. Cultured bacterial isolates from Leg 201 sediments. Species listed are type species from GenBank database.

Closest relative (16S rRNA sequence similarity)	Numbers of isolates (lowest and highest depth of discovery)						
	Open Pacific sites			Peru margin sites			
	1231	1225	1226	1227	1228	1229	1230
				α-Proteobacteria			
Rhizobium radiobacter (98%)		7 (1 to 198 mbsf)	2 (1 to 381 mbsf)	14 (12 to 102 mbsf)		5 (12 to 70 mbsf)	13 (1 to 124 mbsf)
Rhodobacter capsulatus (95%)*							1 (268 mbsf)
Rhodovulum sulfidophilum (96%)	1 (43 mbsf)						
				Firmicutes			
Bacillus firmus (97%)	14 (2 to 43 mbsf)		12 (1 to 420 mbsf)	8 (1 to 102 mbsf)		34 (1 to 187 mbsf)	
Bacillus simplex (96%)*			1 (1 mbsf)			1 (70 mbsf)	
Alkaliphilus transvaalensis (96%)*						4 (1 mbsf)	
Paenibacillus glucanolyticus (98%)		1 (198 mbsf)					
				γ-Proteobacteria			
Vibrio mediterranei (99%)	1 (101 mbsf)				6 (1 to 114 mbsf)	11 (1 to 187 mbsf)	
Vibrio diazotrophicus (99%)*					1 (114 mbsf)		4 (1 to 82 mbsf)
Photobacterium fischeri (94%)					1 (1 mbsf)		
Psychrobacter okhotskensis (98%)							3 (1 to 124 mbsf)
Marinobacter aquaeolei (95%)							1 (268 mbsf)
Marinobacter excellens (98%)*							2 (268 mbsf)
				Actinobacteria			
Micrococcus luteus (98%)		2 (1 to 307 mbsf)	1 (381 mbsf)				
Kocuria palustris (99%)				4 (21 to 40 mbsf)			
Oerskovia paurometabola (92%)	3 (2 to 101 mbsf)			5 (40 to 55 mbsf)			
				δ-Proteobacteria			
Desulfomicrobium norvegicum (99%)*		2 (103 mbsf)					
				Bacteroidetes			
Porphyromonas endodontalis (86%)		1 (198 mbsf)					

*Species names identify the type species in the GenBank database that are the closest relatives of the cultured isolates. The genetic distance between each cultured taxon and its closest relative is illustrated by the percent similarity of their 16S rRNA sequences.

broad array of redox environments and other taxa that appear to exhibit consistent preferences for specific subseafloor environments. At least some of the former taxa are cosmopolitan in their distribution. This broad distribution is not entirely surprising, given (i) the occurrence of so many of the same metabolic products and reactants at every site, (ii) the suitability of spore-forming bacteria for broad dispersal, and (iii) the possibility that individual taxa are responsible for different activities under different subseafloor conditions (*10*).

Much remains to be learned about life in subseafloor sediments. We do not yet know which organisms (cultured or uncultured) are responsible for which metabolic activities in these sediments. We have probably not yet reached the greatest sedimentary depths that subseafloor organisms attain. Their effects on global biogeochemical cycles and their effects on mineral, chemical, and biological resources are poorly constrained. The minimum energy fluxes required to sustain them remain unknown. Their total genetic diversity, rates of population turnover, detailed metabolic interactions, and community structures remain to be determined.

References and Notes

1. R. J. Parkes, B. A. Cragg, P. Wellsbury, *Hydrogeol. Rev.* **8**, 11 (2000).
2. K.-G. Zink, H. Wilkes, U. Disko, M. Elvert, B. Horsfield, *Org. Geochem.* **34**, 755 (2003).
3. H. F. Sturt, R. E. Summons, K. J. Smith, M. Elvert, K.-U. Hinrichs, *Rapid Commun. Mass Spectrom.* **18**, 617 (2004).
4. S. D'Hondt, S. Rutherford, A. J. Spivack, *Science* **295**, 2067 (2002).
5. W. B. Whitman, D. C. Coleman, W. J. Wiebe, *Proc. Natl. Acad. Sci. U.S.A.* **95**, 6578 (1998).
6. S. D'Hondt *et al.*, *Proc. ODP Init. Rep. 201* [CD-ROM] (2003).
7. The youngest sediments are from the seafloor. The oldest sediment is from the base of the sediment column at Peru Basin site 1231; its age is estimated to be late Eocene on the basis of planktic microfossil biostratigraphy (*6*).
8. Leg 201 microbiological studies relied on samples that had very low or undetectable contamination, as assessed by our contaminant tracing tests (*17*).
9. P. N. Froelich *et al.*, *Geochim. Cosmochim. Acta* **43**, 1075 (1979).
10. K. H. Nealson, *Annu. Rev. Earth Planet. Sci.* **25**, 403 (1997).
11. B. B. Jørgensen, in *Marine Geochemistry*, H. D. Schulz, M. Zabel, Eds. (Springer-Verlag, Berlin, 2000), pp. 173–207.
12. H. D. Schulz, in *Marine Geochemistry*, H. D. Schulz, M. Zabel, Eds. (Springer-Verlag, Berlin, 2000), pp. 85–128.
13. E. Suess *et al.*, *Proc. ODP Init. Rep. 112* (1988).
14. P. A. Baker, P. M. Stout, M. Kastner, H. Elderfield, *Earth Planet. Sci. Lett.* **105**, 522 (1991).
15. T. J. Bralower *et al.*, *Proc. ODP Init. Rep. 198* [CD-ROM] (2002).
16. Traces of dissolved O_2 were detected at the top and bottom of the site 1225 and site 1231 sediment columns (*6*). These data were too few and too imprecise to use for estimating O_2 fluxes (*17*).
17. See supporting data on *Science* Online.
18. From alteration textures and chemical traces, prokaryotic life has been inferred to occur in the glassy

rinds of oceanic basalts (*21*). Fe and S in subseafloor basalts are strongly oxidized in the first 10 million to 20 million years of the basalts' existence (*22*). Oxidation of these chemical species has the potential to support abundant biomass in basaltic aquifers (*22*, *23*). Our results indicate that by 11 Ma and 35 Ma at sites 1225 and 1231, respectively, such oxidation is insufficient to strip dissolved O_2 and NO_3^- from the circulating water, perhaps because the mineral surfaces in contact with water were largely oxidized when the basalt was younger.

19. At each site, the sediment column for which fluxes were calculated spans the interval from 1.5 mbsf to a point midway between the two deepest sample depths. At the open-ocean sites, this interval ends just above the sediment-basalt contact. Given an exponential decline in average cell concentrations with depth (*1*), more than 99% of the total biomass in sediments deeper than 1.5 mbsf lies within our calculational interval at each site.
20. Two moles of C(0) (organic carbon) are oxidized by reducing one mole of SO_4^{2-} to S^{2-}. Five moles of C(0) are oxidized by reducing four moles of NO_3^- to two moles of N_2. Four moles of Fe(III), or two moles of Mn(IV), are required to oxidize one mole of C(0).
21. M. R. Fisk, S. J. Giovannoni, I. H. Thorseth, *Science* **281**, 978 (1998).
22. W. Bach, K. J. Edwards, *Geochim. Cosmochim. Acta* **67**, 3871 (2003).
23. T. Gold, *Proc. Natl. Acad. Sci. U.S.A.* **89**, 6045 (1992).
24. R. A. Jahnke, *Global Biogeochem. Cycles* **10**, 71 (1996).
25. K. B. Sørensen, A. Lauer, A. Teske, *Geobiology*, in press.
26. J. Süß, B. Engelen, H. Cypionka, H. Sass, *FEMS Microbiol. Ecol.*, in press.
27. A. Lauer, A. Teske, *Int. J. Astrobiol.* **3** (S1), 63 (2004).
28. Samples, shipboard facilities, and expedition support were provided by the ODP. The NASA Astrobiology Institute (NAI) supported postcruise analysis of biogeochemical data and precruise development of shipboard biogeochemical techniques. Postcruise culturing studies were supported by grants from the Deutsche Forschungsgemeinschaft. We thank three anonymous reviewers for very helpful comments.

Supporting Online Material
www.sciencemag.org/cgi/content/full/306/5705/2216/DC1
Materials and Methods
References

7 June 2004; accepted 15 October 2004
10.1126/science.1101155

REPORTS

Electron Coherence in a Melting Lead Monolayer

F. Baumberger,* W. Auwärter,† T. Greber, J. Osterwalder‡

We used angle-resolved photoemission spectroscopy to measure the electronic dispersion and single-particle spectral function in a liquid metal. A lead monolayer supported on a copper (111) surface was investigated as the temperature was raised through the melting transition of the film. Electron spectra and momentum distribution maps of the liquid film revealed three key features of the electronic structure of liquids: the persistence of a Fermi surface, the filling of band gaps, and the localization of the wave functions upon melting. Distinct coherence lengths for different sheets of the Fermi surface were found, indicating a strong dependence of the localization lengths on the character of the constituent atomic wave functions.

The transition from the solid to the liquid state can have substantial effects on a material's electronic properties (*1*, *2*). In the case of semiconducting germanium, for example, the forbidden states in the band gap of the crystal are filled and the melt is metallic (*3*, *4*). Understanding the evolution of the electronic wave functions, which underlie such marked changes of the physical properties, represents a prime experimental and theoretical challenge. The main conceptual issue is the lack of any long-range order in liquid or amorphous materials. The periodicity of crystalline solids allows the classification of electronic wave functions as Bloch states (i.e., plane waves, modulated by lattice periodic functions, that extend through the entire crystal). In random systems, such as amorphous solids or liquids, the crystal momentum is no longer a good quantum number and the problem becomes analytically intractable (*1*, *5*, *6*).

Despite decades of intense research, many fundamental problems of the electronic structure of liquids remain unresolved (*7*). In particular, the character of the electronic wave functions (e.g., to what extent they are itinerant or localized) has eluded experimental investigation. The primary experimental problem is the loss of periodicity, which restricts the information provided by the most important experimental probes. A diffraction experiment, which can retrieve the full three-dimensional (3D) atomic structure of a crystalline material, yields only a 1D projection in the form of a pair-correlation length in a liquid or amorphous material (*8*). Analogously, angle-resolved photoemission spectroscopy (ARPES), which gives direct access to the single-particle spectral function $A(k,\omega)$ in crystals, only measures the projection of the momentum-resolved quantity on the energy coordinate (i.e., the spectral density) in a liquid.

Recently, it has been shown in an x-ray diffraction experiment that this limitation can be overcome by working on the interface of a liquid and a crystalline material, which led to the first experimental observation of the fivefold local symmetry (*9*), predicted for monatomic 3D liquids more than 50 years ago (*10*). We use a similar idea to directly measure the electron dispersion and spectral function in a 2D liquid: melted Pb. A crystalline Cu(111) substrate serves as a support with minimal influence on the atomic arrangement of the 2D Pb liquid, and at the same time ensures that the parallel momentum of the initial Pb states is conserved in the photoemission process. In a crystalline environment, the momentum needed for photoemission is supplied in discrete quantities by reciprocal lattice vectors, whereas in a liquid, the photoelectrons gather arbitrary momenta in the process. For a liquid monolayer, however, the momentum of the initial state can be retrieved, because the proximity of the crystalline substrate allows transfer of reciprocal lattice vectors to the liquid states.

Complete momentum distribution maps of the liquid film indicate two Fermi surface sheets, and the spectral function (measured independently for both sheets) reveals novel aspects of the electronic structure of liquids. Contrary to the usual assumptions that accompany the concept of a mobility edge, we find only a negligible energy dependence of the localization length (spatial extension of an exponentially decaying wave function) but a marked momentum dependence. This is interpreted as a manifestation of the different symmetries of the constituent atomic orbitals.

The experiments were performed in a modified VG-ESCALAB 220 spectrometer (*11*) using He Iα radiation (21.22 eV). The energy and angular resolutions were set to 60 meV and ±0.4°, respectively. Pb was evaporated resistively onto a clean Cu(111) surface held

Physikinstitut der Universität Zürich, Winterthurerstrasse 190, CH-8057 Zürich, Switzerland.

*Present address: Department of Applied Physics, Stanford University, Stanford, CA 94305, USA.
†Present address: Department of Physics and Astronomy, University of British Columbia, Vancouver, British Columbia V6T1Z4, Canada.
‡To whom correspondence should be addressed. E-mail: osterwal@physik.unizh.ch